Track reconstruction using the TSF method for the BESIII main drift chamber*

LIU Qiu-Guang(刘秋光)[1,2;1)] ZANG Shi-Lei(臧石磊)[3;2)] LI Wei-Guo(李卫国)[1] MAO Ze-Pu(毛泽普)[1]
BIAN Jian-Ming(边渐鸣)[1,2] CAO Guo-Fu(曹国富)[1,2] CAO Xue-Xiang(曹学香)[1,2] CHEN Shen-Jian(陈申见)[5]
DENG Zi-Yan(邓子艳)[1] FU Cheng-Dong(傅成栋)[4,1] GAO Yuan-Ning(高原宁)[4] HE Kang-Lin(何康林)[1]
HE Miao(何苗)[1,2] HUA Chun-Fei(花春飞)[6] HUANG Bin(黄彬)[1,2] HUANG Xing-Tao(黄性涛)[11]
JI Xiao-Bin(季晓斌)[1] LI Fei(李飞)[1] LI Hai-Bo(李海波)[1] LI Wei-Dong(李卫东)[1]
LIANG Yu-Tie(梁羽铁)[7] LIU Chun-Xiu(刘春秀)[1] LIU Huai-Min(刘怀民)[1] LIU Suo(刘锁)[8]
LIU Ying-Jie(刘英杰)[1] MA Qiu-Mei(马秋梅)[1] MA Xiang(马想)[1,2] MAO Ya-Jun(冒亚军)[7]
MO Xiao-Hu(莫晓虎)[1] PAN Ming-Hua(潘明华)[9] PANG Cai-Ying(庞彩莹)[9] PING Rong-Gang(平荣刚)[1]
QIN Gang(秦纲)[1,2] QIN Ya-Hong(秦亚红)[6] QIU Jin-Fa(邱进发)[1] SUN Sheng-Sen(孙胜森)[1]
SUN Yong-Zhao(孙永昭)[1,2] WANG Ji-Ke(王纪科)[1,2] WANG Liang-Liang(王亮亮)[1,2]
WEN Shuo-Pin(文硕频)[1] WU Ling-Hui(伍灵慧)[1] XIE Yu-Guang(谢宇广)[1,2] XU Min(徐敏)[10]
YAN Liang(严亮)[1,2] YOU Zheng-Yun(尤郑昀)[7] YU Guo-Wei(俞国威)[1]
YUAN Chang-Zheng(苑长征)[1] YUAN Ye(袁野)[1] ZHANG Bing-Yun(张炳云)[1]
ZHANG Chang-Chun(张长春)[1] ZHANG Jian-Yong(张建勇)[1,12] ZHANG Xue-Yao(张学尧)[11]
ZHANG Yao(张瑶)[1] ZHENG Yang-Heng(郑阳恒)[2] ZHU Ke-Jun(朱科军)[1]
ZHU Yong-Sheng(朱永生)[1] ZHU Zhi-Li(朱志丽)[9] ZOU Jia-Heng(邹佳恒)[11]

1 (Institute of High Energy Physics, CAS, Beijing 100049, China)
2 (Graduate University of Chinese Academy of Sciences, Beijing 100049, China)
3 (University of Colorado, Boulder, Colorado 80309, USA)
4 (Tsinghua University, Beijing 100084, China)
5 (Nanjing University, Nanjing 210093, China)
6 (Zhengzhou University, Zhengzhou 450001, China)
7 (Peking University, Beijing 100871, China)
8 (Liaoning University, Shenyang 110036, China)
9 (Guangxi Normal University, Guilin 541004, China)
10 (Department of Modern Physics, University of Science and Technology of China, Hefei 230026, China)
11 (Shandong University, Jinan 250100, China)
12 (CCAST(World Laboratory), Beijing 100080, China)

Abstract We describe the algorithm to reconstruct the charged tracks for BESIII main drift chamber at BEPCII, including the track finding and fitting. With a new method of the Track Segment Finder (TSF), the results of present study indicate that the algorithm can reconstruct the charged tracks over a wide range of momentum with high efficiency, while improving the robustness against the background noise in the drift chamber. The overall performances, including spatial resolution, momentum resolution and secondary vertices reconstruction efficiency, etc. satisfy the requirements of BESIII experiment.

Key words BESIII detector, track reconstruction, track segment finder, conformal transformation, secondary vertex

PACS 07.05.kf, 19.85.+c

Received 27 September 2007, Revised 12 December 2007

* Supported by CAS Knowledge Innovation Project (U-602, U-34), National Natural Science Foundation of China (10491300, 10491303, 10605030) and 100 Talents Program of CAS (U-25, U-54)

1) E-mail: liuqg@ihep.ac.cn

2) E-mail: slzang@pizero.colorado.edu

1 Introduction

The BESIII[1] is a high precision, general purpose detector designed for the high luminosity e^+e^- collider running at the tau-charm energy region, called BEPCII[2]. The physics program of the BESIII experiment includes light hadron spectroscopy, charmonium and charm physics, QCD and hadron physics, tau physics and search for new physics, etc. The BESIII detector consists of the main drift chamber (MDC), the electromagnetic calorimeter (EMC), the time of flight counters (TOF), the muon counter (MUC) and the 1 T super-conducting magnet.

The BESIII tracking chamber, located in a 1 T magnetic field, is designed to be small-cell, low-mass drift chamber operated using a $He/C_3H_8(60/40)$ gas mixture. It provides solid angle coverage at $-0.93 \leqslant \cos\theta \leqslant 0.93$, good momentum resolution in a range of 0.1—2 GeV/c, and efficient tracking down to 50 MeV/c. The inner radius and outer radius of the chamber are 64 and 819 mm respectively; its length ranges from 774 mm for the innermost layer to 2400 mm for the outermost layer. The almost square shaped drift cells are arranged in 43 circular layers, which are aligned successively with 8 stereo layers, 12 axial layers, 16 stereo layers and 7 axial layers. From inner to outer, every 4 layers considered as a superlayer, and the outermost superlayer contains 3 axial layers particularly. The cell size is about 12 mm × 12 mm for the 8 inner layers, and about 16.2 mm × 16.2 mm for the following 35 layers. The designed spatial resolution and dE/dx resolution are 130 μm and 6%, respectively. The momentum resolution is expected to be 0.5%@1 GeV/c[3].

Compared with BES II [4], tracking at BESIII will be very challenging due to the requirements of efficient tracking down to very low momentum with high resolution of tracking parameters, while under much higher chamber occupancy in the high luminosity environment. The MDC has been designed and built to meet this important goal, and the track reconstruction software algorithm has to do the same. In this paper, we will describe the track reconstruction software algorithm and show how we improve the algorithm in order to meet these challenges.

2 Tracking at BESIII

The charged particles, created by e^+e^- annihilation, traverse the drift chamber and produce electron-ion pairs along their paths. The ionization electrons, enforced by the electric fields in each cell, drift toward the anode wires. By measuring the drift time for these ionization electrons, the distance between the track trajectory and the anode wire can be determined. Based on the series of position and drift distance of anode wires, these track trajectories can be reconstructed; their curvatures give information on the momentum of the charged particles. The overall track reconstruction software package is based on a similar (earlier version) package from the Belle experiment, with one main improvement developed by us and is tailored for BESIII experiment. The Belle package is based on the so-called Histogram method, in which the track segments are grouped in each superlayer based on the ϕ information of hit wires. Recent studies have shown that the Histogram-based algorithm, when applied to the BESIII case, suffers from the low efficiency at low momentum and its performance is sensitive to high chamber occupancy due to background hits. In order to improve its performance, we proposed and developed the Track Segment Finder (TSF) based algorithm, in which both the position and drift distance of hit wires are considered.

Figure 1 shows the general concept of the TSF-based tracking flow at BESIII. Generally speaking, tracking is a combination of track finding and fitting. After figuring out the track segments in the conformal plane by the Track Segment Finder (TSF), the charged tracks are firstly found in the $r\phi$ plane using axial hit wires and fitted by circle fitting. Then, they are reconstructed in the 3D space using both stereo and axial hit wires. Track parameters are finally determined by helix fitting. The corrections due to energy loss and non-uniformity of the magnetic field are taken care of by a subsequent software package, for simplicity, we will not discuss that in this paper.

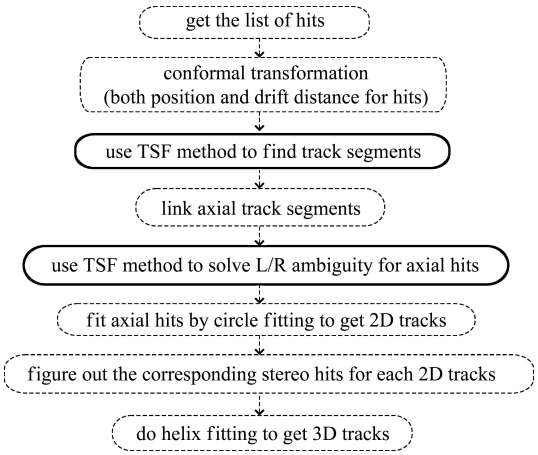

Fig. 1. The TSF-based tracking flow at BESIII.

In order to understand the TSF method, it is convenient to introduce the conformal transformation to help develop a better view of the relation between tracks and hits.

2.1 Conformal transformation

In conformal transformation, as shown in Fig. 2, a hit position (x,y) in xy plane ($r\phi$ plane) is transformed into a position (X,Y) in the conformal plane as,

$$X=\frac{2x}{x^2+y^2},\quad Y=\frac{2y}{x^2+y^2}. \tag{1}$$

Through the conformal transformation, a circle which passes through the origin (0,0) is transformed into a line,

$$x_{\rm c}X+y_{\rm c}Y=1\ , \tag{2}$$

where, $x_{\rm c}$, $y_{\rm c}$ are the center of the circle. The inverse of the distance between the line and the origin in the conformal plane corresponds to the radius of the circles. Meanwhile, a circle which does not pass through the origin in the xy plane is transformed into a new circle. The new circle, still does not pass through the origin in the conformal plane,

$$\left(X-\frac{2x_{\rm c}}{x_{\rm c}^2+y_{\rm c}^2-R^2}\right)^2+\left(Y-\frac{2y_{\rm c}}{x_{\rm c}^2+y_{\rm c}^2-R^2}\right)^2=\left(\frac{2R}{x_{\rm c}^2+y_{\rm c}^2-R^2}\right)^2, \tag{3}$$

where, $x_{\rm c}$, $y_{\rm c}$ and R are the center and the radius of the circle in the natural plane, respectively.

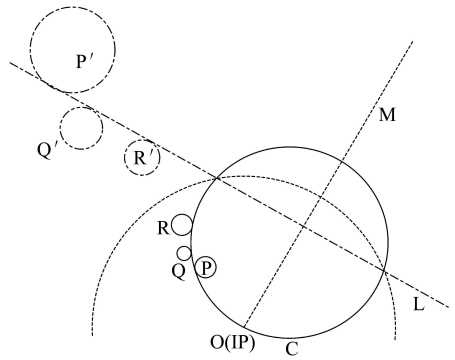

Fig. 2. After conformal transformation, the circle C which passes O(IP) is transferred into line L; the circles P, Q and R which do not pass O are transferred into new circles P′, Q′ and R′.

From the discussions above, it is clear that the tracks coming from the Interaction Point(IP) are represented by lines in the conformal plane, while the drift circles[1)] along a given track are transformed into new circles. These new circles are tangent to the line of the track in the conformal plane. With this in mind, we will describe the TSF method below.

2.2 Track segment finder

Typically, a valid segment pattern consists of hits contiguous in space and time. As we have mentioned, the drift circle of valid hit for a given track is tangent to the line of the track in the conformal plane. If a hit does not belong to this track, its drift circle in the conformal plane would not necessarily be tangent to the line of this track. This unique feature can be used to reject background hits at the track finding stage.

There are four layers within one superlayer. To allow inefficiency of a given layer, 3 out of 4 layers are required to have hits for a given track segment within a superlayer. The track segment finding thus can start either from a cell at the inner most layer (layer 0) or the second layer (layer 1) next to it in case the inner layer does not have a hit due to inefficiency. Therefore, there are two combinations: 4 out of 4 and 3 out of 4, as shown in Fig. 3(a). Fig. 3(b) shows the group in the conformal plane where the range of the area is represented by two dashed-lines. The TSF algorithm starts from the inner most hit first, with a line fitted for each outer layer hit circle to the inner layer hit circle in the conformal plane, resulting in multiple potential lines as shown in Fig. 3(c). To determine which line represents the valid track segment, the hit information from the two middle layers is then used. The lines tangent to the drift circles in the two middle layers are the potential line for a track. Fig. 3(d) shows a valid track segment found using this method.

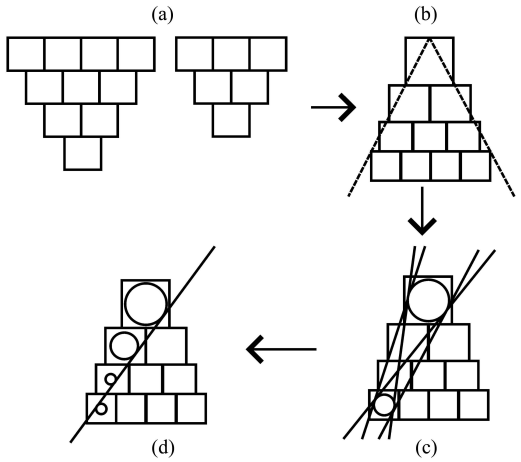

Fig. 3. (a) Two original types of TSF model are defined; (b) Four-layer type pattern in the conformal plane; (c) Four lines are fitted out by the drift circles of the inner and outer hits; (d) With the other hits in this model, whose drift circle can be appended on these lines in some conditions, a track segment is constructed.

As will be shown later, the TSF method described above not only makes the algorithm more robust against high random background hits in the chamber due to beam related background or electronics noises,

1) Represent the hit wires; a circle has its wire position as the center and its drift distance as the radius.

but also makes it less sensitive to low $p_{\rm t}$ tracks curving within the chamber producing multiple circles of hits alone the z direction (the so called curlers). This is because the drift circles from the later stage of the curler are no longer tangent to the original track in the conformal plane, due to energy loss, etc. Therefore, those hits will unlikely cause confusing to the reconstruction of the original track (thus not affecting the tracking efficiency), although redundant or more tracks could be reconstructed from them due to the nature of the curler.

One additional benefit of the TSF method is that it allows one to solve the left-right ambiguity of drift distance. In Fig. 2, the drift circles that are located on the same side of the track will be transformed into the same side in the conformal plane. Consequently, the left-rightness is kept after the conformal transformation.

2.3 Track finding

Track finding part follows that from the Belle reconstruction package, with the exception of using the TSF to solve the left-right ambiguity. Tracks are first found in the $r\phi$ plane when only the axial segments are used. Due to the characteristics of conformal transformation, the segments which belong to the same track have similar directions in the conformal plane. Therefore, the segments are linked by their positions and directions. After solving the left-right ambiguity using the TSF method, a list of 2D tracks can be found using these linked segments with a non-iterative circle fitter[5].

To reconstruct 3D track, the corresponding stereo segments that locate near the 2D track and satisfy a coarse direction restriction, are identified first. The positions of the stereo segments, represented by the wire position with the smallest drift distance, are fitted to obtain the initial lines. Together with the parameters provided by the circle fitting and line fitting, the final 3D tracks are reconstructed using helix fitting, which is described below.

2.4 Helix fitting

The helix fitting part is kept the same as in the Belle reconstruction package. Just for completeness, we include the description here as well. The trajectories of charged particles in uniform magnetic field can be described as a helix. The position (x,y,z) along the helix is given by[6]

$$\begin{cases} x = x_0 + d_\rho\cos\phi_0 + \dfrac{\alpha}{\kappa}\{\cos\phi_0 - \cos(\phi_0+\phi)\} \\ y = y_0 + d_\rho\sin\phi_0 + \dfrac{\alpha}{\kappa}\{\sin\phi_0 - \sin(\phi_0+\phi)\} \\ z = z_0 + d_z - \dfrac{\alpha}{\kappa}\tan\lambda\cdot\phi, \end{cases} \quad (4)$$

where α is the magnetic-field-constant, $\alpha = 1/cB = 10000/2.9979258/\mathrm{B}$ [cm (GeV/c)$^{-}$1] at the strength of magnetic field B [k Gauss], ϕ is the turning angle, that is an internal parameter with a sign, (for instance, ϕ has a negative sign for out-going positive tracks from the pivot.) and determines the location (Fig. 4).

Consequently, the helix can be described by five parameters $a = (d_\rho, \phi_0, \kappa, d_z, \tan\lambda)^{\rm T}$;

1) d_ρ is the signed distance of the helix from the pivot in x-y plane.

2) ϕ_0 is the azimuthal angle to specify the pivot with respect to the helix center.

3) κ is $1/P_{\rm t}$ and the sign of κ represents the charge of the track assigned by the track fitting.

4) d_z is the signed distance of the helix from the pivot in the z direction.

5) $\tan\lambda$ is the slope of the track, tangent of the dip angle.

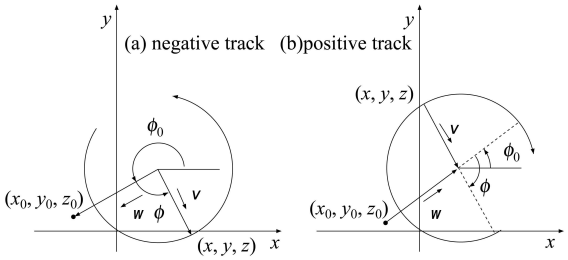

Fig. 4. Schematic representation of the helix parametrization for (a) negative and (b) positive charged track. The vectors in the figure are defined by $\boldsymbol{x} = \boldsymbol{x}_0 + (d_\rho + \rho)\cdot\boldsymbol{w} - \rho\cdot\boldsymbol{v}$, where $\boldsymbol{w} = (\cos\phi_0, \sin\phi_0)^{\rm T}$ and $\boldsymbol{v} = (\cos(\phi_0 + \phi), \sin(\phi_0+\phi))^{\rm T}$.

Least Square Method is used to do the helix fitting. χ^2 is defined as

$$\chi^2 = \sum_{i=1}^{\rm nhits}\left(\frac{drift_i - doca_i}{\sigma_i}\right)^2, \quad (5)$$

where, $drift_i$ means the drift distance to the hit wire, doca means the distance of the closest approach and σ means the error of the drift distance.

We minimize this χ^2 using the Newton Method[7]. The fitted helix parameter a can be numerically found by iterative calculation as follows.

$$a_{(D+1)} = a_{(D)} - \left(\frac{\partial^2\chi^2}{\partial a^{\rm T}\partial a}\right)^{-1}_{(D)}\left(\frac{\partial\chi^2}{\partial a}\right)_{(D)}. \quad (6)$$

The error matrix for helix is described as,

$$E_a = \left(\frac{1}{2}\frac{\partial^2\chi^2}{\partial a^{\rm T}\partial a}\right)^{-1}. \quad (7)$$

3 Performance of tracking algorithm

According to the current schedule, BESIII will start taking beam data at the summer 2008. To

study the performance of the tracking algorithm, at present, we use Monte Carol events. Monte Carlo events are generated by BOOST[8], which is based upon Geant4[9]. For the Monte Carlo events, the average spatial resolution is 122 μm; the dip angle $\cos\theta$ ranges at (−0.93,0.93). The average wire efficiency is assumed to be 98%, taken from the beam test results of the prototype chamber[3]. The noise model of the drift chamber is based upon the studies from BES II [10]. The general tracking performance, such as track reconstruction efficiency, the momentum and spatial resolution, and the robustness against background occupancy have been studied for the TSF based tracking algorithm. In addition, a comparison of the tracking performance between the TSF method and the Histogram method is also presented.

3.1 Efficiency

Track reconstruction efficiency is the primary performance indicator of the algorithm, and is sensitive to the factors such as the number of layers a track passes, the dip angle of track and the noise in tracker, etc. The reconstruction efficiency is defined as,

$$\varepsilon = N_{\rm rec}/N_{\rm mc} \ , \tag{8}$$

where $N_{\rm rec}$ is the number of reconstructed 'good' tracks[1)], and $N_{\rm mc}$ is the number of charged tracks generated in Monte Carlo. Most final state particles in BESIII physics have momentum less than 1 GeV/c; the average momentum is about 0.5 GeV/c. The minimum $p_{\rm t}$, for a charged particle to reach the barrel edge (outer most layer) of the drift chamber, is about 0.12 GeV/c. The ability to reconstruct charged particles with low $p_{\rm t}$ is very important for BESIII physics research. For the track reconstruction efficiency study, we use single μ events with $p_{\rm t}$ ranging from 0.05 GeV/c to 0.5 GeV/c.

The track efficiency versus $p_{\rm t}$ is shown in Fig. 5(a), with the results from both the TSF and the Histogram methods. The efficiency of Histogram method drops significantly for $p_{\rm t}$ below 0.1 GeV/c, while the efficiency of the TSF method is still high even for $p_{\rm t}$ as low as 0.06 GeV/c. This is good because 0.05 GeV/c is the minimum $p_{\rm t}$ at which the charged tracks can only travel 2 stereo superlayers and 1 axial superlayer. Note that the efficiency of the TSF method exceeds 100% in the $p_{\rm t}$ range below 0.12 GeV/c, this is due to the fact that the tracks curling up in MDC could be reconstructed redundantly (the redundant tracks can be removed at a later stage, which will be described elsewhere). The performance using the TSF method is much better than the Histogram method in the low $p_{\rm t}$ range.

We use $J/\psi \to \mu^+\mu^-$ to study the effect of dip angle. the result using the TSF method is shown in Fig. 5(b). Clearly, the track reconstruction efficiency is high and stable, with only a small drop at very large dip angles.

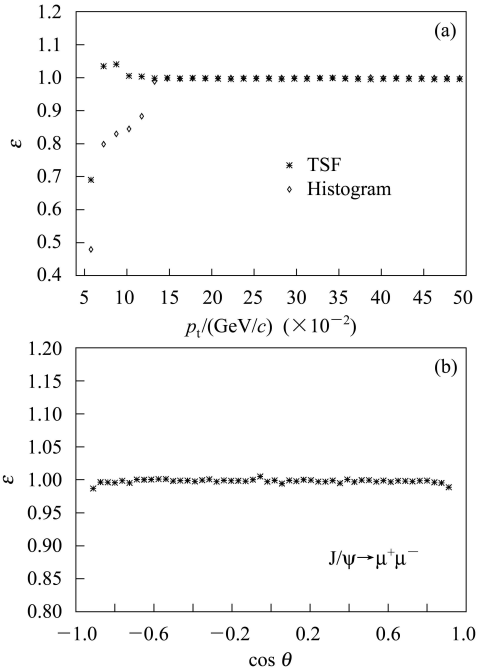

Fig. 5. (a) Efficiencies versus $p_{\rm t}$ for μ using the TSF method and the Histogram method, respectively; (b) Efficiencies versus dip angle for $J/\psi \to \mu^+\mu^-$ using the TSF method.

3.2 Momentum and spatial resolution

The momentum resolution is mainly infected by the position resolution and multiple scattering. In BESIII, the expected momentum resolution is described as

$$\sigma_{p_{\rm t}}/p_{\rm t} = (0.32\%p_{\rm t}) \oplus (0.37\%/\beta) \ . \tag{9}$$

The first term on the right-hand side is the effect of position resolution; the second term is the effect of multiple scattering. Fig. 6(a) shows the momentum resolution versus $p_{\rm t}$. For $p_{\rm t}$ larger than 0.3 GeV/c, the momentum resolution of the reconstructed tracks is somewhat better than the expectation (dashed line).

The spatial resolution is represented by the distribution of the residual, defined as $\Delta d_i = drift_i - doca_i$ and is shown in Fig. 6(b). The plot is fitted by double Gaussians, with

$$\langle\sigma\rangle = \sqrt{\frac{A_1\sigma_1^2 + A_2\sigma_2^2}{A_1 + A_2}} \ , \tag{10}$$

where A_i and σ_i are the area and width of the two Gaussians. For the channel $J/\psi \to \mu^+\mu^-$, the spatial resolution is about 111.4 μm, consistent with our expectation.

1) More than 51% layers in a MC-track have the corresponding hits in the reconstructed track.

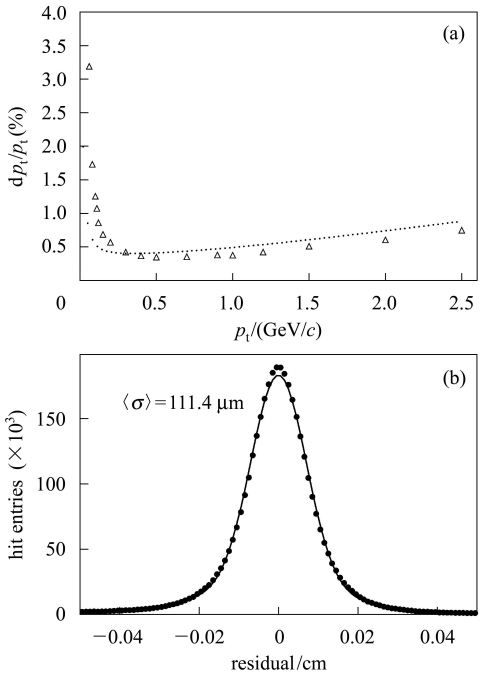

Fig. 6. (a)The p_t resolution of μ on different p_t, in which the dashed line is the expected p_t resolution for μ; (b) the spatial resolution of $J/\psi \to \mu^+\mu^-$ is about 111.4 μm.

3.3 Background hits rejection

The background hits in the drift chamber mainly come from the detector, electronics and beam related background such as the lost particles or synchrotron radiation, etc. Compared with BESⅡ, the drift chamber in BESⅢ is located closer to the beam pipe. As a result, the beam background is expected to be higher and likely dominates the background noise. The background hits make efficient tracking harder, and can significantly affect both the momentum and the spatial resolution if not taken care of. A good tracking algorithm needs to be robust against high background occupancy in the chamber. To study the robustness of the tracking algorithm against high background hits, single μ with p_t at 1 GeV/c and 200 MeV/c, combined with different noise levels are used. The noise level is defined as the ratio of noise occupancy in the first superlayer. For instance, Table 1 shows the noise distribution in each superlayer (SL), when the noise level equals 10%.

Table 1. The distribution of noise in level = 10%.

index of SL	ratio of noise(%)
1	10.0
2	7.0
3—4	4.4
5	2.0
6—11	1.0

Figure 7(a) shows the effect of background noise level on the tracking efficiency, between the TSF method and the Histogram method. Clearly, the TSF-based tracking algorithm is more robust against the background noise level over the Histogram method, with the efficiency still better than 95% when the noise level reaches as high as 60%.

Figure 7(b) shows the momentum resolution versus the noise level for the TSF method. Even with the noise level at 60%, the momentum resolution for μ at 200 MeV/c and 1 GeV/c are 0.46% and 0.57%, respectively.

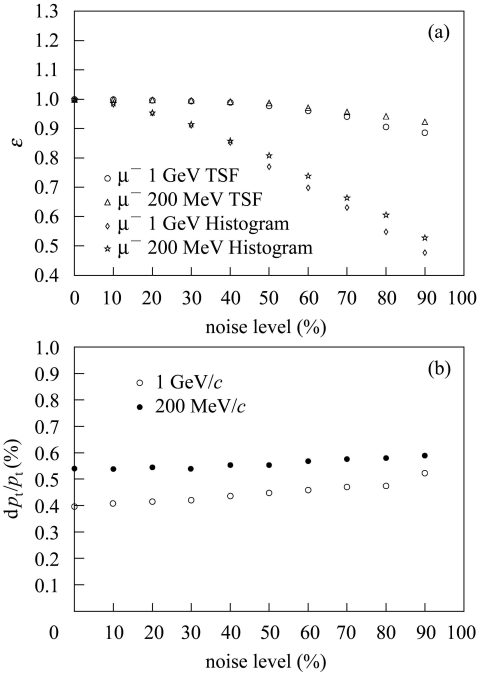

Fig. 7. (a) Efficiencies versus the noise level using the TSF method and the Histogram method, respectively; (b) The p_t resolutions versus the noise level for the TSF method.

3.4 Speed of track reconstruction algorithm

The luminosity of BEPCⅡ is about $10^{33}\mathrm{cm}^{-2}\cdot\mathrm{s}^{-1}$, which means more than 10^{10} events will be accumulated per year. Therefore, improving the CPU time spent on the track reconstruction is essential. We study $J/\psi \to \mu^+\mu^-$ in the farm of lxslc01 in IHEP. The mean CPU time spent on the track reconstruction is currently about 9.83 ms per track, already close to the requirements of BESⅢ experiment and there is room for improvement in the future.

3.5 Application in physics analysis

To further study the performance of tracking, the typical decay channel of $\psi(2S) \to \pi^+\pi^- J/\psi$, $J/\psi \to \mu^+\mu^-$ is used. Final states in this channel are all charged particles $\pi^+\pi^-\mu^+\mu^-$. According to the kinematic characteristics in this process(with decay parent $\psi(2S)$ created at rest), the J/ψ can be seen not only directly from the invariant mass of $\mu^+\mu^-$, but also indirectly from the recoiling mass of $\pi^+\pi^-$.

Since the reconstructed momenta of $\pi^+\pi^-$ and $\mu^+\mu^-$ are used in the invariant mass calculation of each pair, we can use this channel to study the momentum resolution of reconstruction in the main drift chamber. Fig. 8 shows the invariant mass distribution for both pairs where the double Gaussian fit is used for the signal peak. The momentum resolutions are about 3.0 MeV and 16.6 MeV for the recoiling mass of $\pi^+\pi^-$ and the invariant mass of $\mu^+\mu^-$, respectively.

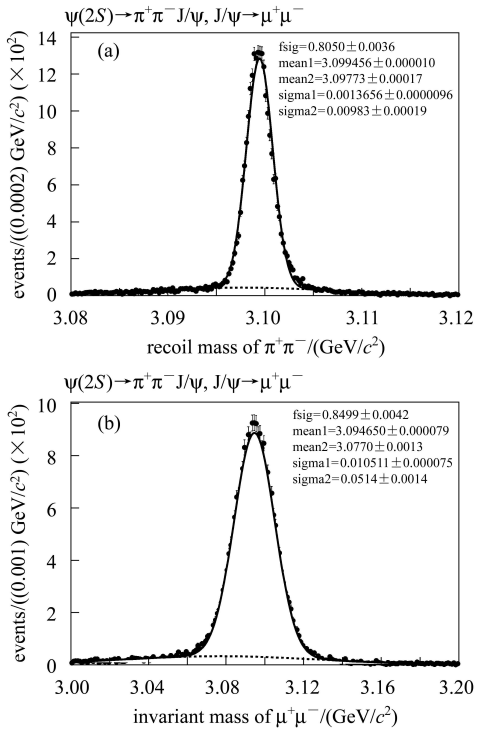

Fig. 8. The channel of $\psi(2S) \to \pi^+\pi^- J/\psi$, $J/\psi \to \mu^+\mu^-$. (a) The recoiling mass spectrum of $\pi^+\pi^-$, the σ of double Gaussian fit is 3.0 MeV; (b) The invariant mass spectrum of $\mu^+\mu^-$, the σ of double Gaussian fit is 16.6 MeV.

To study the tracking performance for decay channels involving secondary vertices, $K_S \to \pi^+\pi^-$ is used. Fig. 9 shows the reconstruction efficiency of the $\pi^+\pi^-$ pair, versus the decay length of K_S. The overall $\pi^+\pi^-$ pair reconstruction efficiency varies slightly around 84%. Considering the coverage limitation of drift chamber (93%), an ideal efficiency of this channel would be nearly 86.5%. Our results show that the current tracking reconstruction works properly for tracks from secondary vertices.

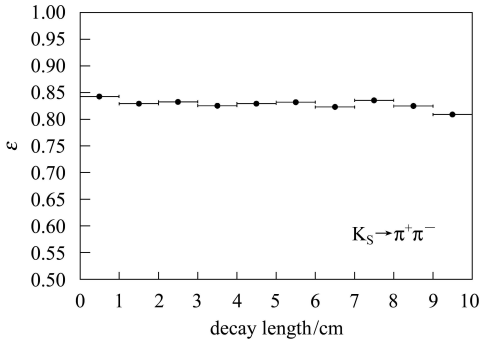

Fig. 9. The efficiency of $\pi^+\pi^-$ reconstruction versus decay length of K_S, in the channel of $K_S \to \pi^+\pi^-$ with momentum of K_S@1 GeV/c.

4 Conclusion

In order to maximize the physics reach at BESIII, it is very important to achieve efficient tracking down to very low momentum with high resolution for the tracking parameters, while under high chamber occupancy in the high luminosity environment. In this paper, we have presented a TSF-based charged track reconstruction algorithm and shown how we have improved the tracking algorithm using the new method in order to meet the tracking challenges at BESIII. The BESIII will start taking beam data during the summer of 2008. In the experimental view, the real data will be much more complex than the Monte Carlo data. Therefore more studies should be done very carefully to improve the algorithm.

The main part of the track fitting program is based on an early version of the transan package from the Belle experiment at KEK, Japan, along with the application of conformal transformation in tracking. We really appreciate all the help from the Belle collaboration.

References

1 WANG Yi-Fang. The Construction of the BESIII Experiment. arXiv:hep-ex/0701010v1
2 BEPC II Preliminary Design Report, 2002
3 LIU Jian-Bei et al. Nucl. Instrum. Methods, A, 2006, **557**: 436—444
4 BAI J Z et al. (BES Collab.). Nucl. Instrum. Methods A, 2001, **458**: 627
5 Crawford J. Nucl. Instrum. Methods, 1983, **211**: 223
6 Ohnishi Y. Track Parametrization, Belle note #148
7 Jun-ichi Tanaka. Fast Tracker For the Drift Chamber, Belle note #222
8 LI Wei-Dong, LIU Huai-Min et al. The Offline Softeware in BESIII Experiment, Proceeding of CHEP06, Mumbai, 2006
9 Agostinelli S et al. (Geant4 Collab.). Nucl. Instrum. Methods A, 2003, **506**: 250
10 DENG Zi-Yan et al. HEP & NP, 2003, **27**(10): 909—913 (in Chinese)